J. Fluid Mech. (2011), *vol.* 687, *pp.* 238–253.
doi:10.1017/jfm.2011.349

Analysis of the melt phase of a rotating polymer disc supporting a diffusion flame

Vedha Nayagam[1]† **and F. A. Williams**[2]

[1] National Center for Space Exploration Research, NASA Glenn Research Center, Cleveland, OH 44135, USA

[2] Department of Mechanical and Aerospace Engineering, University of California at San Diego, La Jolla, CA 92093, USA

(Received 1 February 2011; revised 27 June 2011; accepted 16 August 2011; first published online 11 October 2011)

When a laminar diffusion flame is established over a spinning, thermoplastic, polymer fuel disc in a quiescent, oxidizing environment, the polymer melts and flows radially outwards, causing some fuel to be lost and not transported to the diffusion flame. The viscosity of the liquid in the melt layer retards the radial flow, thereby determining the amount of fuel lost. The melt layer is analysed here for two limiting cases, namely one in which the liquid viscosity depends strongly on temperature, leading to an asymptotic analysis involving two zones in the liquid, and one in which the liquid viscosity is constant, independent of temperature, so that there is only one zone in the liquid. The utility of these two limits is assessed by comparing their predictions with those of full numerical integrations for poly(methyl methacrylate) (PMMA) discs burning in air at atmospheric pressure.

Key words: laminar reacting flows, solidification/melting

1. Introduction

Ever since the discovery by von Kármán (1921) of an exact solution to the Navier–Stokes equations for the flow adjacent to a circular disc rotating steadily about its axis, there has been interest in these von Kármán rotating flows from many different viewpoints (Sparrow & Gregg 1960; Zandbergen & Dijkstra 1987; Kim, Libby & Williams 1992; Nayagam & Williams 2000*b*; Urzay, Nayagam & Williams 2011). While most of the investigations have focused on the flow in the gas phase, liquid-phase flow sometimes also is relevant (Wang 1989, 2007). For example, spiral diffusion-flame patterns on a spinning fuel disc were first seen (Nayagam & Williams 2000*b*) in experiments with poly(methyl methacrylate) (PMMA), a polymer that melts at a glass transition temperature and flows outwards radially somewhat in the liquid phase during combustion. This liquid-phase flow can develop instabilities that introduce departures from axisymmetry at the periphery of the disc. In experiments with PMMA, such instabilities were observed by Hostler, Nayagam & Williams (2000) to lead to elongated fingers extending radially outwards from the edge of the disc. Descriptions of the liquid-phase flow in the polymer melt layer are needed if such instabilities are to be properly addressed theoretically. The objective of the present

† Email address for correspondence: v.nayagam@grc.nasa.gov

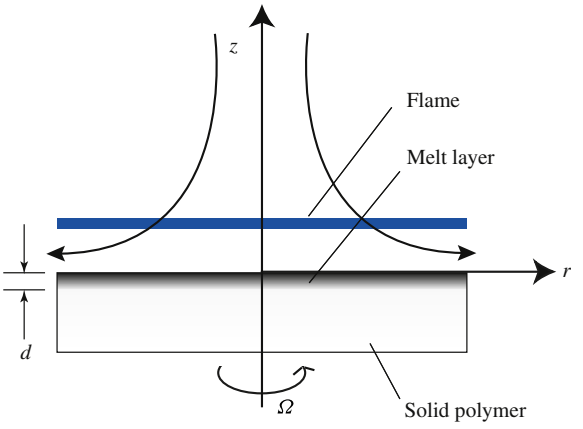

FIGURE 1. (Colour online available at journals.cambridge.org/flm) Schematic illustration of the experiment.

work is to derive suitably simplified descriptions of the liquid-phase flow in these Kármán-swirl experiments that may enable stability analyses to be pursued relatively easily.

The combustion processes themselves for rotating fuel discs in quiescent oxidizing ambient atmospheres occur in the gas phase and have been studied both theoretically (Holcomb & T'ien 1996; Nayagam & Williams 2000*a*; Nayagam, Balasubramaniam & Williams 2009) and experimentally (Balakrishnan 1992; King, Nayagam & Williams 2000) in the past. The influences of the melt layer on the surface of the disc were addressed by Nayagam *et al.* (2009), to which reference can conveniently be made for information concerning properties of the liquid. In that paper, the coupled self-similar ordinary differential equations describing both the gas phase and the condensed phase were solved numerically. Such numerical solutions force numerical methods to be employed when studying the instability patterns observed by Hostler *et al.* (2000). Since the necessity of treating the liquid phase numerically can complicate the task of analysing the instability and can tend to obscure the critical underlying physical processes controlling the phenomena, it is desirable to seek simplified descriptions of the liquid phase, as is done in the present work. In investigating the utility of simplifications that enable liquid-phase solutions to be obtained analytically, it is found here that such simplifications can produce reasonably accurate results for a number of quantities of interest.

2. The gas-phase formulation and liquid-phase properties and energetics

Figure 1 illustrates the thermoplastic polymer disc, occupying a semi-infinite space and rotating about its axis of symmetry with an angular velocity Ω, in a quiescent, oxidizing environment. It is assumed that a steady, laminar diffusion flame is established in the boundary layer above the disc in the gas phase, and a polymer melt layer of thickness d that is to be determined is formed at its surface through the heat transfer from the combustion process. In the coordinate system illustrated in figure 1, the melt–gas interface is located along the plane $z = 0$. In this coordinate system, the spinning solid translates at a steady rate in the positive z direction, corresponding to its melting rate.

2.1. *The gas-phase equations*

With the small effect of radiant energy transport in these blue flames neglected, the conservation equations for mass, momentum, energy and species mass fractions in the gas phase can be reduced to a set of nonlinear ordinary differential equations (see e.g. King *et al.* 2000) by introducing the independent variable

$$\eta = \left(\frac{\Omega}{\nu_\infty}\right)^{1/2} \int_0^z \left(\frac{\rho}{\rho_\infty}\right) \mathrm{d}z' \quad \text{for } 0 \leqslant z \leqslant \infty \tag{2.1}$$

and the dependent variables

$$u = \Omega r F(\eta), \quad v = \Omega r G(\eta), \quad \rho w = \rho_\infty \sqrt{\Omega \nu_\infty}\, H(\eta), \tag{2.2}$$

$$\tilde{T} = \frac{T}{q/c_p}, \quad \tilde{Y}_F = Y_F, \quad \tilde{Y}_O = Y_O/\sigma, \tag{2.3}$$

$$Q = \frac{\tilde{Y}_O - \tilde{Y}_F + \tilde{Y}_{F0}}{\tilde{Y}_{O\infty} + \tilde{Y}_{F0}} = \frac{\tilde{Y}_O + \tilde{T} - \tilde{T}_0}{\tilde{Y}_{O\infty} + \tilde{T}_\infty - \tilde{T}_0}, \tag{2.4}$$

where (u, v, w) are the velocity components in the (r, θ, z) directions, T is the temperature, Y_F is the fuel mass fraction, Y_O is the oxidizer mass fraction, Q is the coupling function, ρ, ν and c_p are the gas-phase density, kinematic viscosity and specific heat, respectively, and q is the heat of combustion per unit mass of fuel vapour consumed. In (2.3), σ is the stoichiometric oxygen-to-fuel mass ratio. Here, the subscripts ∞ and 0 identify conditions far away from the disc and at the melt–gas interface, respectively.

The conservation equations, in terms of these variables, become

$$H' + 2F = 0, \tag{2.5}$$

$$F'' - HF' - F^2 + G^2 = 0, \tag{2.6}$$

$$G'' - HG' - 2FG = 0, \tag{2.7}$$

$$Q'' - Pr_g H Q' = 0, \tag{2.8}$$

where $Pr_g = \nu_\infty/\alpha_\infty$ is the gas-phase Prandtl number, and α is the thermal diffusivity of the gas. The prime in (2.5)–(2.8) denotes differentiation with respect to η. In deriving these equations, the product of density and viscosity, $\rho\mu$, Pr_g and c_p are assumed constant, and the Lewis number is set equal to unity. Also, a one-step, infinite-rate, irreversible reaction in the gas phase is considered, and the conservation equations for the fuel mass fraction $\tilde{Y}_F$, the scaled oxygen mass fraction $\tilde{Y}_O$ and energy have been combined to form a single equation in terms of the coupling function Q defined in (2.4).

From the definitions, the boundary conditions at infinity for (2.5)–(2.8) are $F(\infty) = 0$, $G(\infty) = 0$ and $Q(\infty) = 1$. In addition, from (2.4), since oxygen does not penetrate the diffusion flame, $Q(0) = 0$. Because the system is of seventh order, three more boundary conditions are needed to determine a unique solution. These additional boundary conditions are obtained from interface conservation equations at the liquid–gas surface, which serve to couple the gas-phase differential equations to the conservation equations for the condensed phase.

2.2. *The liquid-phase viscosity and temperature*

In general, the melt layer formed over a burning thermoplastic polymer behaves as a non-Newtonian fluid with a shear-rate-dependent dynamic viscosity. The melt viscosity

strongly depends on its molecular weight as well as on the temperature, as explained, for example, by Brydson (1981). In the present work it is assumed that the melt layer behaves as a Newtonian fluid with a dynamic viscosity μ_l that may or may not vary with temperature. When a temperature variation is considered, this variation is taken to be given by an Arrhenius equation of the form $\mu_l = A\mathrm{e}^{E/RT}$, where A is a constant, E is the activation energy, R is the universal gas constant and T is the absolute temperature. Justification for this last approximation is given by Brydson (1981), for example.

The melt begins at a glass transition temperature T_g (Nayagam *et al.* 2009), located at a distance d from the melt–gas interface, so that introduction of a suitable non-dimensional temperature variable θ in the melt layer, defined to be 0 at T_g and 1 at T_0, enables the liquid temperature to be expressed as $T = T_g + (T_0 - T_g)\theta$. When there is a strong increase of the liquid viscosity with increasing temperature, it is convenient to treat

$$\varepsilon = RT_0^2/[E(T_0 - T_g)] \tag{2.9}$$

as a small parameter, whence the normalized melt viscosity, $\tilde{\mu} = \mu_l(T)/\mu_l(T_0)$, becomes, after a little algebra,

$$\tilde{\mu} = \exp\{(1-\theta)/\varepsilon[1 - (1-\theta)(T_0 - T_g)/T_0]\}, \tag{2.10}$$

an expression that is appropriate for treatment of the melt layer in an expansion for small ε. In the opposite limit of constant liquid viscosity, $\tilde{\mu} = 1$.

In contrast to our earlier work (Nayagam *et al.* 2009), the liquid-phase velocity components (u_l, v_l, w_l) in the (r, θ, z) directions are scaled here on the basis that the rotating disc is nearly in solid-body rotation and experiencing a mass loss rate per unit area in the normal direction that is of the same order as the mass flux in the z direction in the gas. This means that u_l is small compared with Ωr, that v_l is nearly equal to Ωr and that

$$w_l = (\rho_\infty/\rho_l)\sqrt{\Omega \nu_\infty}\, H(0) h, \tag{2.11}$$

where h is of order unity. This definition has been selected so that, by mass conservation at the surface, $h = 1$ at the liquid–gas interface, in view of (2.2), while h will approach a constant value, h_∞, deep within the condensed phase, a value that will be greater than unity because of the mass loss radially from the melt layer. The fraction of the liquid that is lost radially thus will be simply

$$l = (h_\infty - 1)/h_\infty. \tag{2.12}$$

Equation (2.11) indicates that the characteristic normal velocity component in the liquid is smaller than that in the gas, $(\Omega \nu_\infty)^{1/2}$, by a factor of the small density ratio (ρ_∞/ρ_l), of the order of 10^{-3}.

Efficient formulation of the liquid-phase problem for small ε is facilitated by first writing the complete outer solution for the condensed phase. In this case, the z component of velocity throughout most of the condensed phase has a constant value determined by h_∞, so that, given the corresponding equation for energy conservation $(\alpha_l \mathrm{d}^2\theta/\mathrm{d}z^2 - w_l \mathrm{d}\theta/\mathrm{d}z = 0)$, with the non-dimensional spatial variable

$$Z = -z/d, \tag{2.13}$$

the temperature profile in the melt is determined at leading order by

$$\theta = (\mathrm{e}^{-\beta_\infty Z} - \mathrm{e}^{-\beta_\infty})/(1 - \mathrm{e}^{-\beta_\infty}), \tag{2.14}$$

where, in view of (2.11), in terms of the (constant) thermal diffusivity α_l of the liquid and the distance between the surface and the glass transition position,

$$\beta_\infty = (\rho_\infty/\rho_l)(\nu_\infty/\alpha_l)H(0)h_\infty d^*, \tag{2.15}$$

in which

$$d^* = d/\sqrt{\nu_\infty/\Omega} \tag{2.16}$$

is the ratio of the thickness of the liquid layer to a characteristic thickness of the gas-phase layer. In the opposite limit of constant liquid viscosity, the variation of the z component of velocity cannot be neglected throughout most of the liquid, and so the more complicated solution

$$\theta = \int_Z^1 \mathrm{e}^{-\beta}\,\mathrm{d}Z' \Big/ \int_0^1 \mathrm{e}^{-\beta}\,\mathrm{d}Z \tag{2.17}$$

is needed, where

$$\beta = d(\rho_\infty/\rho_l)\sqrt{\Omega\nu_\infty}\,H(0)\int_0^Z h\,\mathrm{d}Z'/\alpha_l. \tag{2.18}$$

2.3. *Incorporation of the influence of the glass transition*

The solution (2.14) can be used to show that the condition of energy conservation across the surface of glass transition (namely, that the rate of heat conduction into that surface from the liquid layer equals the sum of the rate of thermal energy convection into that surface from the solid and the rate of heat absorption in the transition) requires that

$$\beta_\infty = \ln(1 + B_m), \tag{2.19}$$

where B_m, a thermodynamic transfer number for melting at the glass transition, is the ratio of the thermal energy difference of the liquid, between the liquid–gas interface and the glass transition, to the aforementioned sum of the thermal enthalpy difference of the solid and the heat of glass transition, namely, $B_m = c_{pl}(T_0 - T_g)/[L_m + c_{ps}(T_g - T_\infty)]$. Given this result, (2.11) and (2.14) then serve to complete the leading-order outer solution to the condensed-phase problem for small ε, in terms of the (still unknown) non-dimensional mass loss rate of the solid, $H(0)h_\infty$, because (2.15) with use of (2.19) then determines d^*, and the outer condensed phase is in solid-body rotation at this order. For constant viscosity, in place of (2.15), it is more convenient to let β_∞ denote the value of β obtained by putting $Z = 1$ in (2.18), resulting in

$$B_m = h_\infty\beta_\infty \mathrm{e}^{\beta_\infty}\int_0^1 \mathrm{e}^{-\beta}\,\mathrm{d}Z \Big/ \int_0^1 h\,\mathrm{d}Z, \tag{2.20}$$

in place of (2.19), since the melt layer no longer is in solid-body rotation. The solution then is coupled to equations for momentum conservation in the melt layer, since the variation of h cannot be neglected throughout the region over which the temperature varies appreciably. For these reasons, the two limiting cases now need to be analysed separately.

3. Derivation of the liquid-phase velocity-field differential equations

The treatments of the velocity fields differ for the limits of constant and strongly temperature-dependent liquid viscosities.

3.1. *A strongly temperature-dependent viscosity*

Since the inner region will be thin in comparison with the outer region for small ε, to define the inner problem, equation (2.14) may be expanded about $Z = 0$, use being made of (2.15) and (2.19) to evaluate $\mathrm{d}\theta/\mathrm{d}Z$ at $Z = 0$ for purposes of matching, and the result may then be substituted into (2.10) to identify an appropriate inner variable as

$$\xi = -(\rho_\infty/\rho_l)\sqrt{\Omega \nu_\infty}\, H(0) h_\infty z(1 + B_m)/(\alpha_l \varepsilon B_m), \tag{3.1}$$

to be used in formulating the inner liquid-phase problem. This is the most convenient choice because (2.10) then becomes simply

$$\tilde{\mu} = \mathrm{e}^{\xi} \tag{3.2}$$

in the first approximation, resulting in a parameter-free viscosity description.

In view of (2.11) and (3.1), liquid-phase mass conservation, $\partial(ru_l)/\partial r + r\partial w_l/\partial z = 0$ dictates the scaling

$$u_l = \Omega r \delta f, \tag{3.3}$$

where

$$\delta = (\rho_\infty \mu_\infty/\rho_{l0}\mu_{l0})\,[H(0)]^2\, h_\infty (Pr_{l0}/\varepsilon)[(1 + B_m)/B_m], \tag{3.4}$$

with the function $f(\xi)$ being of order unity, so that, with a prime denoting differentiation with respect to ξ in the liquid, conservation of mass in the melt layer becomes simply

$$h' = 2f. \tag{3.5}$$

In (3.4) the liquid Prandtl number based on its viscosity evaluated at the liquid–gas interface is $Pr_{l0} = \mu_{l0}/\alpha_l$. The balance in (3.5) is essential if mass loss in the radial direction is to occur in the melt layer. The excellent approximation $v_l = \Omega r$ replaces conservation of the azimuthal component of momentum in the liquid, and conservation of the normal component serves only to determine the pressure profile in the normal direction, so it is only the conservation of the radial component of momentum,

$$\frac{\partial}{\partial z}\left(\nu_l \frac{\partial u_l}{\partial z}\right) - w_l \frac{\partial u_l}{\partial z} + \frac{v_l^2 - u_l^2}{r} = 0, \tag{3.6}$$

that remains to be considered.

When use is made of (2.11) and (3.1)–(3.3), along with $v_l = \Omega r$, it is found that (3.6) in non-dimensional form is

$$(\mathrm{e}^{\xi} f')' + (\delta^2 h f' + 1 - \delta^2 f^2)/\gamma = 0, \tag{3.7}$$

where

$$\gamma = 4h_\infty^3/a, \tag{3.8}$$

in which

$$a = \left(\frac{4}{[H(0)]^4}\right)\left(\frac{\rho_l \mu_{l0}}{\rho_\infty \mu_\infty}\right)^2 \left(\frac{\varepsilon}{Pr_{l0}}\right)^3 \left(\frac{B_m}{1 + B_m}\right)^3. \tag{3.9}$$

The Prandtl number of the liquid is large (of the order of 10^4 for PMMA of low molecular weight (LMW-PMMA), to 10^7 for PMMA of high molecular weight (HMW-PMMA); see Nayagam *et al.* 2009), but despite the appearance of this factor in δ in (3.4), this parameter is small, as it must be for u_l to be small compared with Ωr, according to (3.3). This occurs because the ratio $(\rho_\infty \mu_\infty / \rho_l \mu_{l0})$ is very small (of the order of 10^{-8} or less, since the ratio of the lowest value of the viscosity of the melt to the viscosity of the gas is of the order of 10^5 at low molecular weight, to 10^8 at high molecular weight, always large compared even with the large density ratio). Thus, the differential equation becomes simply

$$f'' + f' = -\mathrm{e}^{-\xi}/\gamma. \tag{3.10}$$

Matching to the outer solution requires f to go to zero as ξ approaches infinity in the solution to (3.10), and f also must satisfy an interface boundary condition at $\xi = 0$. In view of (3.5) and the boundary condition for h at $\xi = 0$, the solution

$$h = 1 + 2\int_0^\xi f \,\mathrm{d}\xi \tag{3.11}$$

may be used to calculate h_∞, thereby giving the fraction of material lost radially, by use of (2.12), once f is found. Equation (3.10) therefore is the only differential equation that needs to be solved for the liquid phase.

3.2. *A constant liquid-phase viscosity*

The variable ξ of (3.1) no longer is relevant when the viscosity is constant in the liquid phase, and a prime therefore is used to denote differentiation with respect to Z instead. In order to recover (3.5), then, the δ in (3.3) must be replaced by

$$\delta = (\rho_\infty / \rho_l) H(0)/d^*. \tag{3.12}$$

Instead of producing (3.7), (3.6) now gives

$$f'' + (\delta^2 h f' + 1 - \delta^2 f^2)/\gamma = 0, \tag{3.13}$$

where

$$\gamma = H(0)\Gamma/\Delta^3, \tag{3.14}$$

in which

$$\Gamma = (\rho_\infty \mu_\infty / \rho_l \mu_l)^2 \, Pr_l^3 \tag{3.15}$$

and

$$\Delta = (\mu_\infty / \mu_l) Pr_l d^*. \tag{3.16}$$

For small δ^2, (3.10) is then replaced by

$$f'' = -1/\gamma, \tag{3.17}$$

while ξ is replaced by Z in (3.11). In both cases, then, the velocity fields in the melt layer can be obtained from solutions to a single second-order ordinary differential equation, but that equation is different in the two limits.

4. Melt–gas interface boundary conditions

It may be recalled that three additional boundary conditions are needed for the gas phase, in addition to those given in the last paragraph of § 2.1. Since (3.10) and (3.17)

are of second order and obey either a matching condition at infinity or a boundary condition at zero, they require one more boundary condition, so it follows that a total of four more independent boundary conditions are needed at the liquid–gas interface. These conditions will come from continuity of the velocity components in the radial and azimuthal directions, energy conservation and conservation of the radial component of momentum across the surface. Conservation of the azimuthal component of momentum across the surface becomes superfluous in the approximation $v_l = \Omega r$, and the additional boundary condition for G then reduces to $G(0) = 1$ from (2.2). From (2.2) and (3.3), continuity of the radial component of velocity results in

$$F(0) = \delta f(0), \tag{4.1}$$

which in the first approximation for small δ is $F(0) = 0$. From (2.1), (2.2) and (3.3), the condition for conservation of the radial component of momentum across the interface, $\mu\, \partial u/\partial z = \mu_l\, \partial u_l/\partial z$, can be shown, by use of the definitions of the non-dimensional coordinates and of δ and γ, in both cases, to be

$$f'(0) = -[F'(0)/H(0)](\delta/\gamma), \tag{4.2}$$

which is $f'(0) = 0$ in the first approximation. Since none of these three additional boundary conditions introduce any coupling between the gas-phase and liquid-phase solutions at leading order, the liquid-phase solutions affect the gas-phase solutions only through the interface energy conservation condition, and they also enable the liquid-phase solutions to be determined prior to addressing the gas-phase problem.

Since radiant energy loss from the surface is negligible (King *et al.* 2000), conservation of energy across the interface requires that the rate of conduction of energy into the surface from the gas equals the sum of the rate of conduction of energy out of the surface into the liquid and the vaporization rate times the latent heat of vaporization. From (2.1)–(2.4), (2.13)–(2.15) and (2.19), this can be shown to reduce to the non-dimensional equation, applicable for small ε,

$$(B/Pr_g)Q'(0) = H(0)[1 + (1 + B_m)(B_l/B_m)h_\infty], \tag{4.3}$$

where B is the usual transfer number defined by Nayagam *et al.* (2009), and B_l is the ratio of the thermal enthalpy difference of the liquid between the liquid–gas interface and the glass transition to its heat of vaporization, another known non-dimensional thermodynamic parameter; specifically, $B = (\tilde{Y}_{O\infty} + \tilde{T}_\infty - \tilde{T}_0)/(L_v/q)$ and $B_l = c_{pl}(T_0 - T_g)/L_v$. Equation (4.3) also can be interpreted as an overall energy balance, saying that the heat conducted into the liquid from the gas goes into causing vaporization of the portion of the liquid that does not escape radially (the first term on the right-hand side) and heating all of the condensed phase from its initial state to liquid at the liquid–gas interface temperature (the last term). For small ε, all of the material that escapes is heated to this temperature in the first approximation, and the additional factor h_∞ in the last term, which finally couples the gas-phase problem to the condensed-phase problem, accounts for the fact that more material is heated than is vaporized. By contrast, when the liquid viscosity is constant, some material escapes radially without being heated entirely to the gas-interface temperature, and (4.3) is modified in that $(1 + B_m)$ is replaced by e^{β_∞}, since (2.19) no longer applies, and the energy transported radially by material loss depends on β_∞. The expression then becomes

$$(B/Pr_g)Q'(0) = H(0)(1 + B_l/B_m) + 2B_l\Delta^3 e^{\beta_\infty}/(3\Gamma B_m). \tag{4.4}$$

5. The liquid-phase solutions

The solution to (3.10), subject to $f'(0) = 0$ and $f(\infty) = 0$, is

$$f(\xi) = [(1 + \xi)/\gamma]\mathrm{e}^{-\xi}, \tag{5.1}$$

which may be used in (3.11) to show that

$$h(\xi) = 1 + 4/\gamma - 2[(2 + \xi)/\gamma]\mathrm{e}^{-\xi}. \tag{5.2}$$

According to (5.2),

$$h_\infty = 1 + 4/\gamma, \tag{5.3}$$

so that from (2.12), the fraction of liquid lost radially is

$$l = 1/(1 + \gamma/4), \tag{5.4}$$

with the γ of (3.8). Equation (5.3) yields

$$h_\infty^3(h_\infty - 1) = a, \tag{5.5}$$

which determines h_∞ in terms of $H(0)$ for the small-ε limit. This quartic equation for h_∞ can conveniently be solved numerically for use in (4.3).

Similarly, for $\tilde{\mu} = 1$, (3.17) may be integrated with $f'(0) = 0$, yielding

$$f = f(0) - Z^2/(2\gamma), \tag{5.6}$$

which, with the obvious additional no-slip boundary condition at the glass transition, $f(1) = 0$, implies that $f(0) = 1/(2\gamma)$. Then, from (3.11),

$$h = 1 + Z(1 - Z^2/3)/\gamma, \tag{5.7}$$

so that $h_\infty = h(1) = 1 + 2/(3\gamma)$, and, from (2.12),

$$l = 1/(1 + 3\gamma/2), \tag{5.8}$$

with the γ of (3.14). The solution for h may be substituted into the expression for β, (2.18), which, in turn, will provide the solution for θ, the non-dimensional temperature in the liquid phase, from (2.17). Since the integral of h from zero to one is $1 + 5/(12\gamma)$, it follows from the expression for β that

$$\beta_\infty = [1 + 5/(12\gamma)]\,\mathrm{d}(\mu_\infty/\mu_l)\sqrt{\Omega/\nu_\infty}\,H(0)Pr_l. \tag{5.9}$$

Use of these last results in (2.20) then provides an expression that, in principle, determines d^* in terms of other parameters, enabling δ and γ to be related to $H(0)$. The modified (4.3) then becomes

$$\left(\frac{B}{Pr_g}\right)Q'(0) = H(0) + \frac{B_l}{B_m}\left[H(0) + \frac{2\Delta^3}{3\Gamma}\right]\mathrm{e}^{\Delta H(0) + (5/12)\Delta^4/\Gamma}, \tag{5.10}$$

with Δ required to satisfy

$$B_m = \left[\Delta H(0) + \frac{2\Delta^4}{3\Gamma}\right]\mathrm{e}^{\Delta H(0) + (5/12)\Delta^4/\Gamma}\int_0^1 \mathrm{e}^{-\Delta H(0)Z - [\Delta^4/(2\Gamma)](Z^2 - Z^4/6)}\,\mathrm{d}Z, \tag{5.11}$$

from (2.20).

6. The gas-phase solution and scalings

Equations (2.5)–(2.8) are to be solved subject to the boundary conditions

$$F_0(\infty) = G_0(\infty) = F_0(0) = Q_0(0) = 0, \quad G_0(0) = Q_0(\infty) = 1, \tag{6.1}$$

and (4.3) for small ε or (5.10) for $\tilde{\mu} = 1$. The liquid-phase solution influences the gas-phase solution through the value of h_∞ in (4.3) for small ε, requiring use of (5.5), and through Δ, determined by (5.11), for $\tilde{\mu} = 1$. Since $H(0)$ appears in (3.9), the solution to (5.5) for h_∞ will introduce nonlinearity into the boundary condition in (4.3). As h_∞ approaches unity (small material loss radially), (4.3) becomes linear, while, when most of the material is lost radially (that is, h_∞ is large), (4.3) becomes

$$\left(\frac{B}{Pr_g}\right) Q'(0) = H(0) + \sqrt{2} B_l \left(\frac{1+B_m}{B_m}\right)^{1/4} \left(\frac{\varepsilon}{Pr_{l0}}\right)^{3/4} \left(\frac{\rho_l \mu_{l0}}{\rho_\infty \mu_\infty}\right)^{1/2}, \tag{6.2}$$

again linear. The problem, however, is simpler for small ε than for $\tilde{\mu} = 1$ because, in using (5.10), it becomes necessary to evaluate the integral in (5.11) numerically, to test whether the gas-phase solution satisfies that equation. The gas-phase solution in principle must be obtained numerically in both limits, although earlier numerical results given by Sparrow & Gregg (1960) could be curve-fitted to provide $Q'(0)$ as a function $H(0)$, which would make it unnecessary to perform numerical integrations.

Nayagam *et al.* (2009) developed approximate scalings in dimensionless parameters concerning dependences of mass loss rates and liquid-layer thicknesses on liquid-phase properties, treating HMW-PMMA and LMW-PMMA separately, representative, respectively, of small and large liquid-layer loss fractions. The present analytical results for small ε shed some light on these scalings. The previously employed mass loss and layer-thickness parameters were, respectively,

$$w_l / \sqrt{\Omega \nu_{l0}} = (\rho_\infty / \rho_l) \sqrt{\nu_\infty / \nu_{l0}}\, H(0) h_\infty \tag{6.3}$$

and $d/\sqrt{\nu_{l0}/\Omega} = d^* \sqrt{\nu_\infty / \nu_{l0}}$, where use has been made of (2.11) and (2.16). Introduction of (2.15) and (2.19) into the last of these expressions results in

$$\frac{d}{\sqrt{\nu_{l0}/\Omega}} = \frac{(\rho_l/\rho_\infty)\sqrt{\nu_{l0}/\nu_\infty}}{h_\infty H(0) Pr_{l0}} \ln\left(1 + \frac{1}{Ja}\right), \tag{6.4}$$

where the Jacob number Ja defined in Nayagam *et al.* (2009) is the reciprocal of the thermodynamic transfer number B_m used in this paper. Explicit scalings can be generated from these formulae in two limiting cases, namely $h_\infty = 1$ and h_∞ large. The HMW-PMMA is closer to the former limit, and from these formulae, in which (4.3) with $h_\infty = 1$ is to be used for $H(0)$, it is seen that both parameters in that limit become proportional to $\nu_{l0}^{-1/2}$, consistent with the previous scaling as $Pr_{l0}^{-1/2}$, since the variation of the Prandtl number was dominated by that of the viscosity. The LMW-PMMA, on the other hand, is closer to the latter limit, for which introduction of (3.9) and (5.5) into these expressions results in

$$\frac{w_l}{\sqrt{\Omega \nu_{l0}}} = \sqrt{2} \left(\frac{\epsilon}{Pr_{l0}}\right)^{3/4} \left(\frac{1}{1+Ja}\right)^{3/4} \tag{6.5}$$

and

$$\frac{d}{\sqrt{\nu_{l0}/\Omega}} = \frac{1}{\sqrt{2}} \frac{Pr_{l0}^{-1/4}}{\epsilon^{3/4}} (1+Ja)^{3/4} \ln\left(1 + \frac{1}{Ja}\right). \tag{6.6}$$

The predicted dependence on Pr_{l0} shown here is the same as in Nayagam *et al.* (2009), while the Ja dependence is somewhat different but approaches the previous $Ja^{-3/4}$ dependence for the mass loss parameter and the $Ja^{-1/4}$ dependence for the liquid-depth parameter when $Ja \gg 1$. Equations (6.4)–(6.6) also provide additional scaling information concerning dependences on other condensed-phase properties and on gas-phase properties in these two limits.

7. The method of computation

Numerical integrations for this problem have been performed previously by Nayagam *et al.* (2009) for two types of PMMA, one (LMW-PMMA) of low molecular weight and the other (HMW-PMMA) of high molecular weight. Values of the physical properties of these two types of PMMA are given in that paper. Although the liquid melt-layer density is listed correctly there as $\rho_l = 1.09$ g cm^{-3}, the calculations actually were performed for $\rho_l = 1.50$ g cm^{-3}. To facilitate comparisons, this last value is also employed here; the differences in results for the two different values are all less than 10 %, and so there is no effect on the conclusions.

For the problem with a strongly temperature-dependent viscosity, first the gas-phase conservation equations (2.5)–(2.8) are solved numerically with the boundary conditions given in (6.1) along with an assumed value of $H(0)$, using the two-point boundary-value-problem solver COLSYS (Asher, Christiansen & Russell 1981), which yields a value for $Q'(0)$, proportional to the heat flux from the gas into the surface. Equation (4.3) is then used to calculate h_∞. These known values $H(0)$ and h_∞ are substituted into (5.5) to obtain an error estimate. Then, using Newton's method, new guesses for $H(0)$ are successively obtained, such that the error in satisfying (5.5) is reduced below a specified limit, taken to be 1×10^{-5} for results presented here. For cases in which h_∞ is large, (6.2) may be used directly as a boundary condition for the gas-phase equations, along with equation (6.1), and $H(0)$ is then calculated without the need for any iterations; in this limit, (5.5) gives h_∞ simply as $a^{1/4}$.

For constant melt-phase viscosity, the solutions proceed in a similar fashion. Equation (5.10) is used as one of the boundary conditions for the gas phase with an initially guessed value for Δ. The resulting solution for $H(0)$ and the guessed Δ are then used in (5.11), with the integral evaluated numerically, to obtain an error estimate. Again, Newton's method is used to improve successive guesses for Δ, such that the error in satisfying (5.11) is reduced below the specified limit.

According to (2.2), $H(0)$ is a non-dimensional measure of the gasification rate, and, while analytical results based on universal solutions can be generated by expansions for small values of $H(0)$ (Urzay *et al.* 2011), the values are not sufficiently small in the present application for those results to be accurate. Hence, as before (Nayagam *et al.* 2009), the gas-phase solutions have to be generated numerically, the only numerical-integration saving here being the very minor one of analytical condensed-phase solutions. This computational saving is more than offset by the need for iterations to satisfy the nonlinear equations. Computationally, therefore, the present investigation is more involved than a simple numerical integration. Its contribution instead lies in increased understanding and in providing analytical condensed-phase solutions that facilitate stability analyses of fingering generation.

8. Comparisons and discussion

Figures 2 and 3 show profiles of the non-dimensional radial velocities $u_l/(\Omega r)$ as functions of the non-dimensional depth z/d in the liquid layer, for the LMW-PMMA

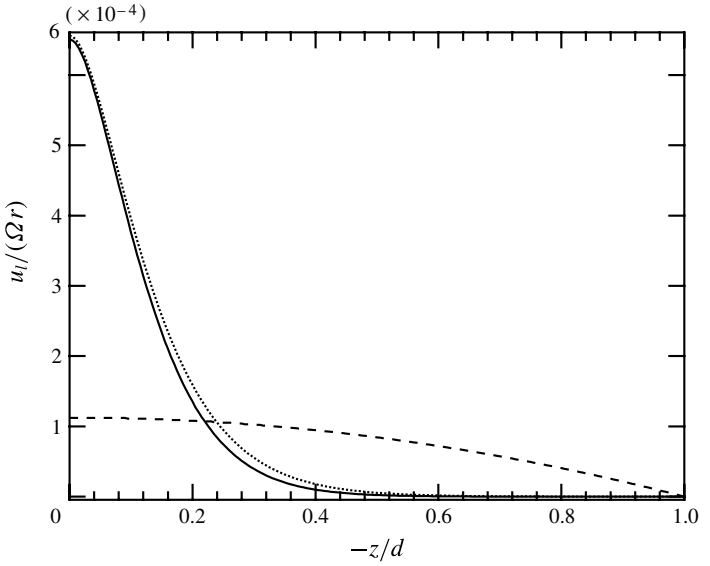

FIGURE 2. Profiles of the radial velocity of the liquid, normalized by the rotational velocity, as functions of the depth, normalized by the liquid-layer thickness, for LMW-PMMA: solid curve, numerical results; dashed curve, constant-viscosity approximation; dotted curve, composite solution generated from asymptotic results.

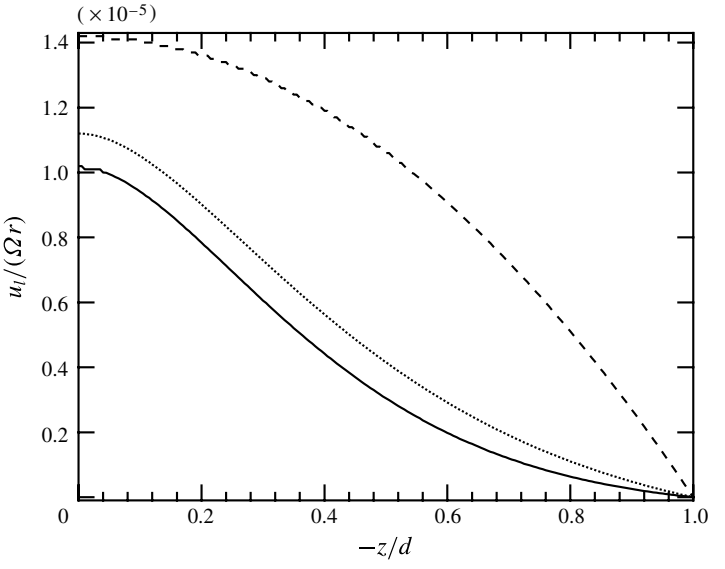

FIGURE 3. Profiles of the radial velocity of the liquid, normalized by the rotational velocity, as functions of the depth, normalized by the liquid-layer thickness, for HMW-PMMA: solid curve, numerical results; dashed curve, constant-viscosity approximation; dotted curve, composite solution generated from asymptotic results.

and HMW-PMMA, respectively, considered previously (Nayagam *et al.* 2009). The radial velocity is selected here because it provides the most information: temperature profiles all agree closely and bow down only slightly from linearity; azimuthal

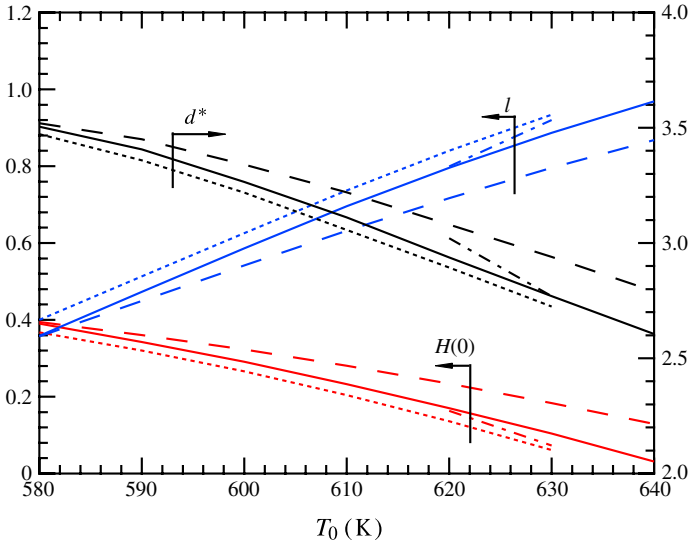

FIGURE 4. (Colour online) Comparisons of liquid-layer thickness, liquid-loss fraction and burning rate for LMW-PMMA: solid curves, earlier numerical results; dashed curves, constant-viscosity approximation; dotted curves, asymptotic results; dot-dashed curves, large mass loss limit of asymptotic results.

velocities are in solid-body rotation; and normal velocities are simply obtained from the radial velocities by integration. The previous numerical results (Nayagam *et al.* 2009), shown by the solid curves, are seen to be very close to the asymptotic results in the dotted curves. The latter were generated by approximating the composite solution as the inner solution from (5.1), minus the common part of the outer solution, taken to be simply the value of the inner solution at $z/d = 1$. While this correction by subtraction would be too small to be seen for LMW-PMMA, it is substantial for HMW-PMMA, for which the value of ε is significantly larger. Unlike the close agreement of the asymptotic and numerical profiles, the constant-viscosity profiles, shown by the dashed curves, obtained from (5.6) employing the constant values identified in the following paragraph, are seen to differ substantially from the numerical results in both cases. This is understandable because they neglect the variation of viscosity with temperature, which strongly influences the profiles. Nevertheless, as indicated below, they still can give fairly reasonable melt-layer mass loss fractions by averaging over the profiles.

Figures 4 and 5 compare the present results, respectively, for LMW-PMMA and HMW-PMMA, with the numerical results of (Nayagam *et al.* 2009) for the dimensionless fuel mass flux $H(0)$ consumed in the gas-phase combustion, the fraction l of liquid melt lost radially and the ratio d^* of the liquid-layer thickness to the gas-layer thickness. In each figure, the dotted lines correspond to asymptotic results obtained for small ϵ, the dot-dashed lines represent the limiting case of asymptotic results for large mass loss occurring along the edges (see (6.2)), the dashed lines are for the constant-viscosity approximation, and the solid lines correspond to the earlier numerical calculation. The results are presented as functions of an assumed surface temperature T_0, which depends on the kinetics of the depolymerization process and increases with increasing gas-phase burning rate, among other things (Kashiwagi, Omori & Nanbu 1990). Although this dependence could be approximated by an

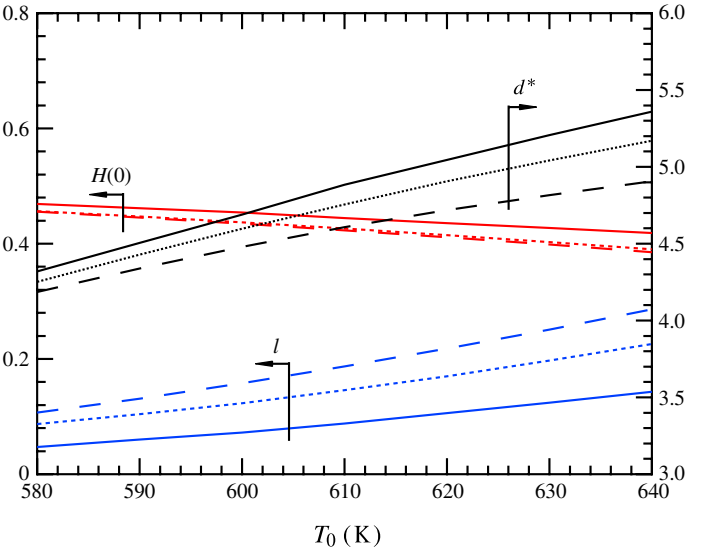

FIGURE 5. (Colour online) Comparisons of liquid-layer thickness, liquid-loss fraction and burning rate for HMW-PMMA: solid curves, earlier numerical results; dashed curves, constant-viscosity approximation; dotted curves, asymptotic results; dot-dashed curves, large mass loss limit of asymptotic results.

Arrhenius expression, and such expressions can be generated for both materials, ultimately relating T_0 to their rotation rates Ω, that would introduce additional physics and functional dependences that would further complicate explanations. Therefore, in an effort to clarify interpretations, a range of surface temperatures is simply selected here, covering experimentally measured values (Kashiwagi *et al.* 1990), as was done earlier for the numerical calculations by Nayagam *et al.* (2009).

The values of the gasification-rate parameter $H(0)$ predicted by the asymptotic solution is seen to be very close to the exact numerical solution but slightly below it, for both types of PMMA. The differences are associated with the value of ϵ of (2.9) not being sufficiently small as assumed; that value, about 0.1 for LMW-PMMA and 0.35 for HMW-PMMA, is consistent with the roughly 10 % differences observed. A value of $H(0)$ that is too small leads to a value of h_∞, proportional to the ratio of the solid consumption rate to $H(0)$ according to (2.11), that is too large, as may be seen, for example, from (3.9) and (5.5), and thereby produces from (2.12) a value of the loss fraction l that is too large, resulting in the over-prediction of loss by the asymptotic analysis, seen in the figures. While the difference remains of the order of 10 % for LMW-PMMA, it becomes nearly a factor of 2 for the HMW-PMMA, which has a higher value of ϵ, leading to greater inaccuracy. This behaviour is understandable because a smaller value of $H(0)$ results in an increased heat flux from the gas phase to the condensed phase as a consequence of the diffusion flame moving closer to the disc surface. This increased heat flux leads to a higher amount of melting compared to the amount of material being burned in the gas phase and proportionately higher amount of mass loss fraction, with the energetic parameters B, B_l and B_m being fixed.

Now we examine why the mass loss fraction in general increases with increasing surface temperature T_0. As we increase the condensed-phase surface temperature, with the gas-phase conditions fixed, it takes more energy to gasify the fuel, and so the

flame moves closer to the fuel surface to maintain steady state. This in turn requires that the mass flux to the gas phase ($H(0)$) be reduced to decrease the blowing effect, and, as explained in the preceding paragraph, a reduction in $H(0)$ leads to an increase in mass loss fraction. Increasing the surface temperature also decreases the liquid viscosity, contributing to an increase in mass loss fraction, though this effect is not as strong as the effect of the increased surface heat flux melting more solid while at the same time burning less in the gas phase. Beyond a surface temperature of about 630 K, where the curves from the asymptotic theory end for LMW-PMMA, the theory predicts a gasification rate $H(0)$ very close to zero and the flame almost collapses to the surface. Under those high-temperature conditions for the LMW-PMMA, then, the melt layer becomes so thin that the constant-viscosity limit is a better approximation. Note that the linearized boundary condition (6.2), applicable in the limit of high mass loss fraction, yields reasonable results only for LMW-PMMA around a surface temperature of 630 K. As expected, this limit is not applicable for HMW-PMMA, for which liquid loss is so small that the layer thickness actually increases with increasing T_0.

Excluding the high temperatures for LMW-PMMA, where the asymptotic analysis is inapplicable, the difference between the asymptotic and numerical predictions of the ratio of melt-layer to gas-layer thickness, d^*, is of the order of 10 %, comparable with that for $H(0)$. That the asymptotics under-predicts the melt-layer thicknesses is understandable because the numerical integrations extend accurately throughout the melt layer, including the deep part near the glass transition where the viscosity is very high. Although the numerical results certainly are more accurate, in applying the results to addressing liquid-phase flow and instabilities, the high-viscosity melt deep within the layer is unlikely to be relevant, and so the analytical results may actually provide a better estimate of the thickness of the layer that should be considered.

In the constant-viscosity calculations, it is necessary to select the temperature at which the viscosity is evaluated, since this temperature affects the predictions strongly. The arithmetic mean of the surface temperature and the glass transition was employed for the results shown in the figures. This is the simplest choice, and trials with other selections, such as weighting with radial flow velocities, proved less satisfactory. If the surface temperature is used, then the predicted loss is much too high, and if the glass transition is used, then there is essentially no loss at all. The selected average is seen in the figures to over-estimate $H(0)$ for LMW-PMMA and to under-estimate it (by the same amount as the asymptotic analysis) for HMW-PMMA. Associated with this is an under-prediction of the loss for the first material and an over-prediction for the second, by a factor of 2 or more in the second instance. The constant-viscosity results thus are inferior for HMW-PMMA, while they tend to be nearly as good as the asymptotic results for LMW-PMMA, and they extend to temperatures beyond which the asymptotics can be applied in that case, albeit with decreasing accuracy that could be improved only by choosing a lower temperature at which to evaluate the viscosity.

9. Conclusions

It may be concluded from this study that analytical descriptions of the behaviour of the melt phase of spinning thermoplastic polymer fuel discs supporting diffusion flames can be developed that yield burning rates and melt-layer flow rates with reasonable accuracy. For most purposes, a two-zone asymptotic analysis treating the temperature dependence of the liquid viscosity as a large parameter produces better results than a one-zone, constant-viscosity approximation, and, moreover, it

leads to a simpler formulation. The asymptotic approach, however, fails at high radial loss rates of liquid in the melt, where the outer zone becomes too thin for the asymptotics to apply. Under such conditions, a constant-viscosity approximation is better, but it suffers from uncertainty concerning the temperature at which the constant viscosity is to be evaluated. The analytical descriptions of the melt phase can facilitate future investigations of melt-layer flow and instabilities that lead to non-axisymmetric patterns.

von Kármán swirling flows arise in many different contexts in fluid mechanics. Combustion processes constitute only one of many examples. There are, however, interesting combustion processes, involving diffusion flames, as well as premixed flames, for which further investigations of this flow configuration can be revealing. Besides polymer melts with finger formation, such investigations could address flame extinction in swirling flow, spiral-flame development and observed meandering of flame motions over fuel surfaces.

This work was supported by the Fire Prevention, Detection, and Suppression Project at the NASA Glenn Research Center and directed by Dr G. Ruff.

REFERENCES

ASHER, U., CHRISTIANSEN, J. & RUSSELL, R. D. 1981 Algorithm COLSYS: collocation software for boundary value ODE's. *ACM Trans. Math. Softw.* **7**, 223–229.

BALAKRISHNAN, M. 1992 An experimental analysis of the laminar burning characteristics of a rotating solid fuel disk. Master's thesis, University of Alabama, Tascaloosa, Alabama.

BRYDSON, J. A. 1981 *Flow Properties of Polymer Melts*, 2nd edn. George Godwin.

HOLCOMB, J. M. & T'IEN, J. S. 1996 Diffusion flame adjacent to rotating solid fuel disk in zero gravity. *AIAA J.* **35**, 742–744.

HOSTLER, S. R., NAYAGAM, V. & WILLIAMS, F. A. 2000 Melt-front instabilities during the combustion of a spinning polymer disk. In *Procedings of the Technical Meeting of the Central State Section of the Combustion Institute*.

VON KÁRMÁN, TH. 1921 Über laminare und turbulente reibung. *Z. Angew. Math. Mech.* **1**, 232–252.

KASHIWAGI, T., OMORI, A. & NANBU, H. 1990 Effects of melt viscosity and thermal stability on polymer gasification. *Combust. Flame* **81**, 188–201.

KIM, J. S., LIBBY, P. A. & WILLIAMS, F. A. 1992 Influence of swirl on the structure and extinction of strained premixed flames. Part II. Strong rates of rotation. *Phys. Fluids* A **4** (2), 391–408.

KING, M. D., NAYAGAM, V. & WILLIAMS, F. A. 2000 Measurements of polymethyl methacrylate diffusion flames in von Karman swirling flows. *Combust. Sci. Technol.* **160**, 151–163.

NAYAGAM, V., BALASUBRAMANIAM, R. & WILLIAMS, F. A. 2009 Diffusion flames over a melting polymer disk in von Karman swirling flows. *Combust. Flame* **156**, 1698–1704.

NAYAGAM, V. & WILLIAMS, F. A. 2000*a* Diffusion-flame extinction for a spinning fuel disk in an oxidizing counterflow. *Proc. Combust. Inst.* **28**, 2875–2881.

NAYAGAM, V. & WILLIAMS, F. A. 2000*b* Rotating spiral edge flames in von Kármán swirling flows. *Phys. Rev. Lett.* **84** (3), 479–482.

SPARROW, E. M. & GREGG, J. L. 1960 Mass transfer, flow, and heat transfer about a rotating disk. *ASME J. Heat Transfer* **81**, 294–302.

URZAY, J., NAYAGAM, V. & WILLIAMS, F. A. 2011 Theory of the propagation dynamics of spiral edges of diffusion flames in von Kármán swirling flows. *Combust. Flame* **158** (2), 255–272.

WANG, C. Y. 1989 Melting from a horizontal rotating disk. *ASME J. Appl. Mech.* **56**, 47–50.

WANG, C. Y. 2007 Condensation film on an inclined rotating disk. *Appl. Math. Model.* **31** (8), 1582–1593.

ZANDBERGEN, P. J. & DIJKSTRA, D. 1987 von Karman swirling flows. *Annu. Rev. Fluid Mech.* **19**, 465–491.